Chapter 11
Neuroreceptor Imaging

Habib Zaidi and Miho Shidahara

Abstract Neuroreceptor imaging using PET and SPECT has contributed to clinical neuroscience and diagnosis (e.g. neurodegenerative disease and antipsychotic-drug receptor occupancy). Recent advances in dedicated PET and SPECT instrumentation, disease-specific radioligands, and image analysis techniques contributed to the further development of this field and its widespread application. In this chapter, we introduce the basis concepts of neuroreceptor imaging using typical radioligands, standard modeling and analysis techniques and discuss future research opportunities in the field.

Keywords Kinetic modeling • PET • Quantification • Receptor imaging • SPECT

11.1 Basic Principles of Neuroreceptor Imaging

11.1.1 Neuroimaging Using PET and SPECT

The last quarter century has witnessed the introduction of a variety of powerful medical imaging technologies allowing the visualization of organ structure and function with exquisite detail. Modern functional brain mapping techniques such as positron emission tomography (PET), single-photon emission computed tomography

H. Zaidi, Ph.D. (✉)
Division of Nuclear Medicine and Molecular Imaging, Geneva University Hospital, CH-1211 Geneva, Switzerland

Geneva Neuroscience Center, Geneva University, Geneva, Switzerland

Department of Nuclear Medicine and Molecular Imaging, University Medical Center Groningen, University of Groningen, Groningen, Netherlands
e-mail: habib.zaidi@hcuge.ch

M. Shidahara, Ph.D.
Division of Medical Physics, Tohoku University Graduate School of Medicine, Sendai, Japan
e-mail: shidahara@med.tohoku.ac.jp

I.-Y. Choi and R. Gruetter (eds.), *Neural Metabolism In Vivo*,
Advances in Neurobiology 4, DOI 10.1007/978-1-4614-1788-0_11,

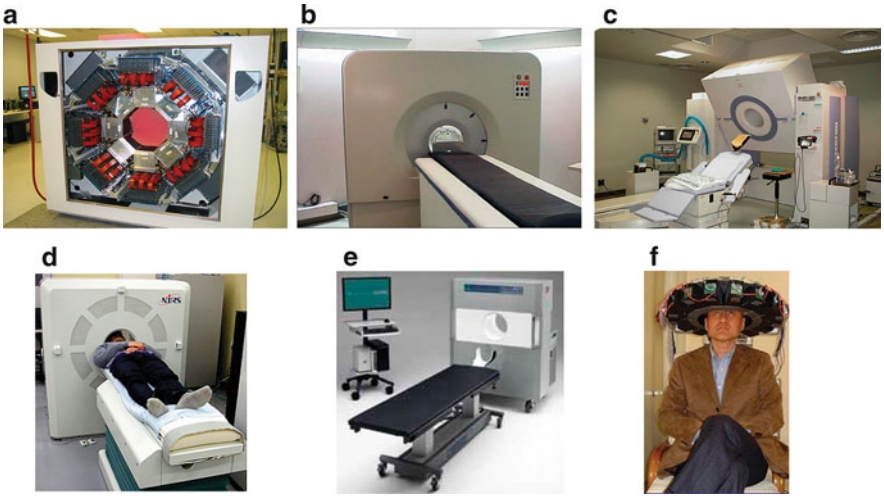

Fig. 11.1 Photographs of dedicated brain PET scanners showing (**a**) the HRRT camera based on LSO scintillation crystals and the phoswich concept, (**b**) the GSO-based PET (G-PET) camera, (**c**) the Hamamatsu SHR-12000 PET scanner based on BGO detector blocks, jPET-D4 brain PET scanner (**d**), the NeuroPET™ (**e**), and the PET-Hat wearable PET system (**f**)

(SPECT), functional magnetic resonance imaging (fMRI), electro-encephalography (EEG), magneto-encephalography (MEG), optical imaging and neuroanatomical tools have been used for assessing the functional organization of the human brain (Gilman 1998; Hammoud et al. 2007). Through these techniques, neuroscience has progressed to a great extent in the understanding of the brain in health and disease.

The specific role of molecular SPECT and PET imaging in the expansion of our understanding of the pathophysiological mechanisms of neurological and psychiatric diseases and in the clinical management of patients is steadily progressing (Jacobs et al. 2003). Both imaging modalities allow *in vivo*, non-invasive three-dimensional (3-D) imaging of regional cerebral blood flow, metabolism and neuroreceptor binding in the brain, amino acid synthesis or amyloid plaque (Heiss and Herholz 2006). Since functional disturbances occur often earlier than structural ones, a faster and more sensitive detection of pathology is possible, compared with anatomical imaging with, for example structural MRI.

During the last two decades, functional brain imaging using SPECT and PET has advanced elegantly and steadily gained importance in the clinical and research arenas. Various clinical indications for molecular neuroimaging using SPECT and PET were adopted and novel applications are being explored. The demand for non-invasive functional, metabolic, and molecular imaging of the brain has stimulated the development of dedicated high-resolution SPECT (Accorsi 2008) and PET (Sossi 2007; Zaidi and Montandon 2006) instrumentation and the synthesis of new radiopharmaceuticals (Fowler et al. 2004; Halldin et al. 2001). Current existing commercial brain PET technology and other dedicated prototype designs constitute state-of-the-art high resolution PET instrumentation dedicated for brain research. Figure 11.1 shows photographs of the some of these designs.

Software- and hardware-based multimodality brain imaging allowing the correlation between anatomical and molecular information has revolutionized clinical diagnosis and now offers unique capabilities for the clinical neuroimaging community and neuroscience researchers at large. To respond to the requirements of emerging clinical and research applications of correlated anatomical and functional brain imaging, several innovative developments in high performance standalone (PET and MRI) and dual-modality PET-MR imaging instrumentation combining both modalities, thus allowing simultaneous or sequential PET and MR brain imaging have been proposed and are currently being assessed in clinical and research settings (Cho et al. 2008; Schlemmer et al. 2008).

This chapter discusses recent advances in neuroreceptor imaging and advanced quantitative imaging procedures in clinical setting. Future opportunities and challenges facing the adoption of neuroreceptor imaging will also be addressed.

11.1.2 Physiological Aspects of Neuroreceptors and Transporters

Receptors are structures, typically proteins, on cellular membranes that, following interaction with specific ligands (first messenger transmitters), activate a signal instigate distinct responses interceded by secondary messengers (G-protein-coupled receptors) as ion channels (ligand-gated ion channels) (Heiss and Herholz 2006). Receptors are usually characterized by their affinity and density and are generally degraded by specific proteases after a functional period. Radioligands are used to visualize and quantify the distribution, density and activity of neuroreceptors.

Apart from indirect cerebral parameters such as metabolism and perfusion, molecular neuroimaging techniques can also offer the unique possibility to image a large set of receptors. Nerve signals pass through synapse between different neurons. This process is a chemical event in which neurotransmitters from the presynaptic nerve terminals are released to the synaptic cleft, and act on the postsynaptic neurotransmitters to induce excitation or inhibition on the target neuron. Through reuptake sites (transporter) on the presynaptic membrane, the surplus in neurotransmitters can be recycled. Changes of important neurotransmitter systems such as the dopamine, GABA (gamma aminobutyric acid), benzodiazepine, choline and serotonin neurotransmitter systems have been demonstrated in many neurological and psychiatric disease stages. For a detailed overview, the reader is referred to Tikofsky et al. (1999).

Receptors play a key role in neurotransmission and neuromodulation and as such are involved in almost all physiological functions of the brain from motor performance to memory, emotion, and pain (Heiss and Herholz 2006). The possibilities offered by molecular imaging to visualize the distribution, density and activity of various receptors open a far-fetched plethora of tools allowing to investigate the physiological activities of functional networks and their disruption by neurologic and psychiatric disorders. In addition, imaging can be efficiently used for assessing selective drug action.

11.2 Radioligands for Neuroreceptor Imaging

11.2.1 Radioligands

The word "ligand" in biochemistry denotes a molecule that binds to a specific protein (e.g. receptor). The distribution, density and affinity of receptors can be visualized and quantified by "radioactive ligands" based on the tracer principle. Over the last three decades, a large number of radioactive ligands have been developed; however, most of them were used only in laboratory animals and primates (e.g. rodents and monkeys). Only a small portion (but not a small number) was introduced and successfully used for human imaging studies (Table 11.1).

Typical isotopes for labeling are ^{11}C (physical half-life $T_{1/2} = 20.4$ min) and ^{18}F ($T_{1/2} = 109.8$ min) for PET and ^{123}I ($T_{1/2} = 13.2$ h) and ^{99m}Tc ($T_{1/2} = 6.01$ h) for SPECT. Although the use of short-lived isotopes for PET and SPECT presents the disadvantage in terms of rapid synthesis requirements, their use enable the administration of a reasonable amount of activity for imaging resulting in a relatively low dose to subjects. In the human body, Carbon is contained within every organic molecule and Iodine is contained within several organic molecules which allow isotopic

Table 11.1 Examples of receptor radioligands for human PET and SPECT studies (Adapted from Halldin et al. 2001)

Binding system	Radioligand	Binding system	Radioligand
Dopamine D_1	[^{11}C]NNC 112	Serotonin transporter	[^{11}C]DASB
	[^{11}C]SCH 23390		[^{11}C]McN5652
			[^{123}I]ADAM
			[^{123}I] β-CIT
Dopamine D_2	[^{11}C]Raclopride	Musacrinic	[^{11}C]MNPB
	[^{11}C]FLB 457		[^{123}I]IQNB
	[^{11}C]MNSP		[^{123}I]IQNP
	[^{11}C]MNPA	Nicotinic	Epibatidine
	[^{18}F]fallypride	Opiate	[^{11}C]diprenorphine
	[^{123}I]epidepride		[^{11}C]carfentenyl
	[^{123}I]IBZM		
Dopamine transporter	[^{11}C]PE2I	Peripheral benzodiazepine	[^{11}C]PK 11195
	[^{11}C]β-CFT		[^{11}C]DAA 1106
	[^{11}C]altropane		[^{11}C]AC-5216
	[^{123}I] β-CIT	Benzodiazepine	[^{11}C]flumazenil
	[^{123}I]PE2I		[^{11}C]Ro15 1788
	[^{99m}Tc]altropane		[^{11}C]Ro15 4513
	[^{99m}Tc]TRODAT-1		[^{123}I]iomazenil
Serotonin 5-HT_{1A}	[^{11}C]WAY 100635	Amyloid	[^{11}C]PIB
Serotonin 5-HT_{2A}	[^{11}C]MDL 100907		[^{11}C]BF 227
	[^{11}C]MNSP		[^{11}C]FDDNP
	[^{18}F]altanserin		[^{123}I]IMPY

labeling. Fluorine and Technetium in general do not occur in biologically important compounds. Ligands labeled with ^{11}C offer the great advantage of making repeated examinations in the same subject on the same day feasible owing to its short half-life. On the other hands, the longer half-lives of ^{18}F, ^{99m}Tc, ^{123}I compared to ^{11}C can be attractive for the study of biological processes with relatively slow kinetics. At present, PET represents the most selective and sensitive method for measuring receptor density and interactions *in vivo*. SPECT can also be applied but the sensitivity is by approximately two or three orders of magnitude lower than PET owing to the use of a physical collimation (Rahmim and Zaidi 2008). Longer half-lives may partially compensate for SPECT disadvantages if measurement times over several hours are required. Furthermore, SPECT also enables simultaneous trace of radioligand behavior in the subject through the combination of several isotopes with different emitting energies (Dresel et al. 1999).

Radioligands for neuroreceptor imaging should satisfy the following criteria: stability of labeling radioisotopes, sufficient nanomolar affinity and high selectivity for the specific receptor with low nonspecific binding in brain tissue, rapid permeation through blood-brain barrier (BBB) (Halldin et al. 2001). Furthermore, metabolites in plasma should be avoided to enter the brain through BBB (Pike 2009).

To increase the selectivity of radioligands to specific binding, low non-specific binding is preferable (Pike 2009). The term "non-specific binding" refers to the binding of a radioligand to the lipid bilayer and is generally proportional to the lipophilicity of the ligand (Rosso et al. 2008). The logarithm of the partition coefficient between buffers accounting for ionization at physiological pH and octanol (log *P*) is often taken as a useful index for the lipophilicity of a compound in the context of biological systems. Conversely, some degree of lipid solubility is needed for passing over the BBB. However, the lipophilic nature of a molecule might also favor binding to plasma proteins, thus reducing the available "free fraction" in blood, which is the fraction of the tracer available for transport into brain tissue. Moreover, lipophilic molecules are also more likely to be extracted and metabolized in lung circulation (Halldin et al. 2001).

11.2.2 Imaging Targets

11.2.2.1 Dopamine Transporters and Receptors

Dopaminergic neurotransmission has a central role in many brain functions. Both pre- and post-synaptic dopaminergic functions can be visualized and quantified through the use of various radioligands (Table 11.1). For the measurement of dopamine D_1 receptor binding, [^{11}C]SCH 23390 (Farde et al. 1987; Halldin et al. 1986) and [^{11}C]NNC 112 (Halldin et al. 1998) are used. On the other hand, dopamine D_2 receptor densities are measured with the low affinity [^{11}C]raclopride in striatum (high D_2 density) and with the high affinity [^{11}C]FLB 457 for extrastriatal low density

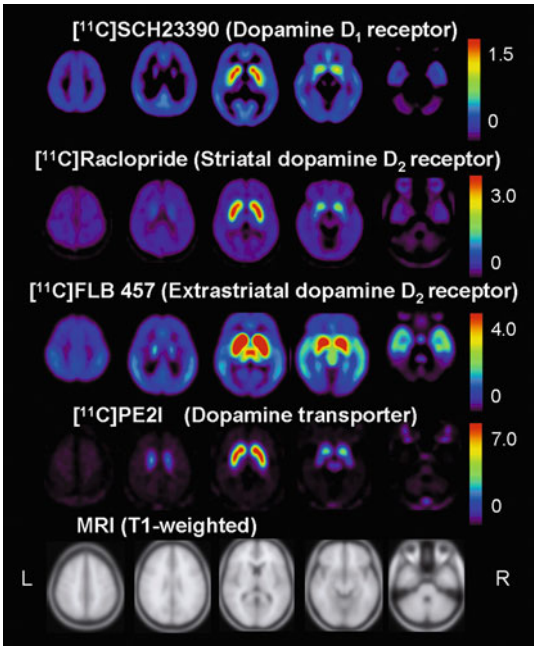

Fig. 11.2 Representative slices of dopaminergic PET imaging using various radioligands: averaged binding potential image of ten young healthy subjects (Data courtesy of Dr. Hiroshi Ito, NIRS)

regions, respectively. Presynaptic dopaminergic function is quantified measuring the dopamine transporter binding with [^{11}C]β-CIT (Farde et al. 1994; Muller et al. 1993), [^{11}C]PE2I (Emond et al. 1997), [^{99m}Tc]TRODAT-1 (Kung et al. 1996), and many others (Brucke et al. 1993) while the endogeneous dopamine synthesis rate can be measured by 6-[^{18}F]fluoro-L-Dopa and L-[b-^{11}C]DOPA (Hartvig et al. 1991). Figure 11.2 demonstrates PET imaging of the dopaminergic system in the human brain that has the highest density in striatum (Ito et al. 2008).

11.2.2.2 Serotonin Transporters and Receptors

Serotonin receptors (5-hydroxytryptamine, 5-HT) and the 5-HT transporter have an important role in affective disorders and for the assessment of the activity of antidepressants. Postsynaptic 5-HT receptor are diversified in 7 major classes containing more than 16 subtypes. Suitable radioligands are only available for 5-HT$_{1A}$ and 5-HT$_{2A}$ subtypes. For the measurement of 5-HT$_{1A}$ receptor binding, the radioligand of choice is [^{11}C]WAY 100635 (Pike et al. 1996). To measure the binding of 5-HT$_{2A}$ receptor, [^{11}C]MNSP (Burns et al. 1984), [^{11}C]MDL 100,907 (Ito et al. 1998b; Lundkvist et al. 1996; Watabe et al. 2000) and [^{18}F]altanserin (Crouzel et al. 1992) are used. Presynaptic 5-HT function, 5-HT transporter binding can be measured with [^{11}C]DASB (Houle et al. 2000; Wilson et al. 2000), [^{123}I] β-CIT (Laruelle et al. 1993), and many other radioligands (Oya et al. 2000; Suehiro et al. 1993). 5-HT transporter belongs to the same family of the transporters for dopamine and

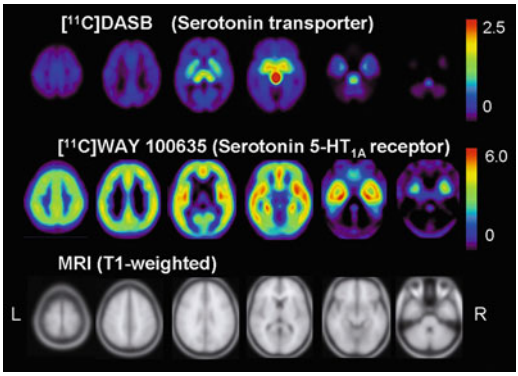

Fig. 11.3 PET images of 5-HT transporter and receptor ligands: averaged binding potential image of 13 young normal subjects (Data courtesy of Dr. Harumasa Takano, NIRS, Japan)

norepinephrine. The distribution and density of a typical 5-HT transporter and receptor is demonstrated in Fig. 11.3.

11.2.2.3 Amyloid Imaging

Excessive amyloid-β (Aβ) deposition in the brain is one of the crucial events in the early pathological state of Alzheimer's disease (AD). PET and SPECT amyloid imaging using a radioligands for Aβ deposit has been paying attention as promising biomarker imaging technique for AD diagnosis (Furumoto et al. 2007). Even though amyloid imaging is not receptor but plaque imaging, here we list several amyloid radioligands, which selectively binds to β-sheet structure of Aβ. [^{11}C]FDDNP is the first radioligand for amyloid imaging (Agdeppa et al. 2003; Shoghi-Jadid et al. 2002), however, [^{11}C]PIB is most widespread. This radioligand is a Thioflavin which is stain analogue to Congo red that sticks to the protein β-sheet (Klunk et al. 2004). Many other radioligands have also been developed, e.g. [^{11}C]BF-227 (Furumoto et al. 2007; Kudo et al. 2007). There are few SPECT radioligands, [123I]IMPY being one of them (Kung et al. 2002). However, the longer half-life of gamma-emitting radionuclides, which allows the delivery of radioligands to virtually all hospitals and facilities, would be strongly beneficial.

11.3 Neuroreceptor Ligand Model

11.3.1 General Considerations

The modeling approach for *in vivo* radioligand binding studies in the brain assumes a compartment model that has at its basis a description of substrate-receptor interactions. The simplest model describing the interaction of a free ligand *L* with a receptor

R to form the complex RL is the interaction between buffer solution and receptor tissue expressed as follows (Michaelis and Menten 1913):

$$L + R \underset{K_{off}}{\overset{K_{on}}{\rightleftharpoons}} RL \tag{11.1}$$

where k_{on} and k_{off} are the association and dissociation constants, respectively. By introducing the equilibrium dissociation constant K_D ($= k_{off}/k_{on}$) and the total number of receptors B_{max} ($= [R] + [RL]$), Eq. 11.1 can be written as:

$$[RL] = \frac{B_{max}[L]}{[L] + K_D} \tag{11.2}$$

Separate estimation of B_{max} and K_D requires saturation analysis where measurements are repeated with increasing amount of ligand and the above referenced parameters obtained by fitting the following formula arranged from Eq. 11.2 (Scatchard 1949).

$$\frac{[RL]}{[L]} = \frac{B_{max} - [RL]}{K_D} \tag{11.3}$$

This model can be adapted into the concept of receptor imaging. If the radioligand is administrated in tracer amounts, then $[RL]$ is very small compared with $[R]$, i.e. $B_{max} \approx [R]$ and Eq. 11.2 can be rearranged as follows:

$$BP = \frac{B_{max}}{K_D} = \frac{[RL]}{[L]} \tag{11.4}$$

where BP is the binding potential defined as the ratio of B_{max}/K_D and is equal to the radio of the concentrations of bound and free radioligand. BP is proportional to B_{max} if K_D is constant.

In case of a PET or SPECT study, radioligands are administered intravenously into the human body, go to the heart, and are then delivered to the target organ by arterial blood. The portion of the radioligand that is exchanged with tissue is the one in plasma not bound to plasma proteins (mainly albumin). From plasma, the radiotracer passes through the BBB into the brain and some portion of the radiotracer binds to specific receptors. Dynamic PET or SPECT data acquisitions consisting in a series of time-frames acquired for a time (1–2 h or more in the case of long-half life isotopes and SPECT) provide accurate measurement of the time-course of the tracer. The kinetics of a radioligand depends on the number of receptors in the target organ, its affinity, the non-specific binding, cerebral blood flow, and the concentration of an endogenous competitor. For estimation of detailed physiological parameters (e.g. receptor density and radioligand affinity to a specific receptor, binding

Table 11.2 Typical parameters in receptor modeling *in vivo* (Adapted from Innis et al. 2007)

Abbreviation	Description	Units
B_{max}	Density of receptors *in vitro*	pmol (mg protein)$^{-1}$
B_{avail}	Density of receptors available to bind radioligand *in vivo*	nmol·L^{-1}
BP	*In vitro* binding potential	
BP_{ND}	*In vivo* binding potential	Unitless
f_p	Free fraction in plasma	Unitless
f_{ND}	Free fraction in nondisplaceable compartment	Unitless
K_1	Rate constant for transfer from arterial plasma to tissue	mL·cm^{-3}·min^{-1}
k_2, k_3, k_4	Rate constants	min^{-1}
K_D (k_{off}/k_{on})	Dissociation constant	nmol·L^{-1}
k_{off}	*In vitro* dissociation rate constant	min^{-1}
k_{on}	*In vitro* association rate constant	nmol·L^{-1}·min^{-1}
V_T	Volume of distribution expressed relative to total plasma ligand concentration C_p	mL·cm^{-3}

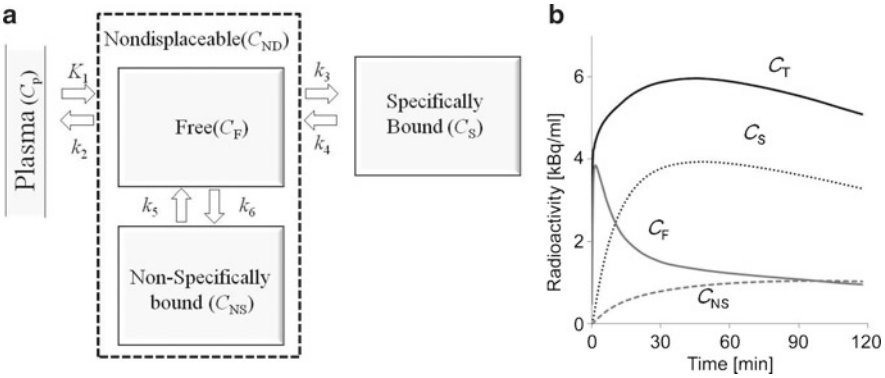

Fig. 11.4 Standard compartmental model for receptor-binding radioligands (**a**) and time courses of radioactivity in each compartment (**b**), where C_T is the total radioactivity concentration in C_S, C_F and C_{NS} compartments, respectively

potential), the application of pharmacokinetic modeling to the tracer time-activity course is required. Table 11.2 summarizes the consensus nomenclature for neuroreceptor imaging that has been adopted since 2007 (Innis et al. 2007).

11.3.2 Standard Reversible Neuroreceptor Model

Depending on each radioligand's kinetics, several compartmental models have been used (Heiss and Herholz 2006; Schmidt and Turkheimer 2002; Watabe et al. 2006; Bentourkia and Zaidi 2007). In this section, we only discuss the standard reversible compartment model shown in Fig. 11.4.

The standard neuroreceptor reversible model in the brain is based on the two-tissue three-compartment model (Fig. 11.4). From arterial blood as a first compartment, the free exchangeable radioligand in plasma passes into the second compartment known as the free compartment. The third compartment is the region of specific binding which we are usually interested to observe. The fourth compartment is a nonspecific binding compartment that exchanges with the free compartment. In practice, for most radioligands, the nonspecific binding compartment is in rapid equilibrium with the free compartment and the two compartments are treated as a single compartment. If the nonspecific binding compartment is considered separately, the compartment model would be much more difficult to solve reliably (Watabe et al. 2006). Exchanges between compartments are governed by simple linear differential equations:

$$\begin{aligned}\frac{dC_{ND}(t)}{dt} &= K_1 C_P(t) - (k_2 + k_3) C_{ND}(t) + k_4 C_S(t) \\ \frac{dC_S(t)}{dt} &= k_3 C_{ND}(t) - k_4 C_S(t) \\ C_T(t) &= C_{ND}(t) + C_S(t)\end{aligned} \tag{11.5}$$

where K_1 [mL·cm^{-3}·min^{-1}] is the rate constant for transfer from arterial plasma to tissue, k_2, k_3 and k_4 [min^{-1}] are rate constants. C_P [Bq cm^{-3}] is the radioactivity concentration of the unchanged radioligand in plasma (arterial input function), C_{ND} [Bq cm^{-3}] is the radioactivity concentration of non-displaceable radioligand in brain (ND: non-displaceable tissue uptake), including nonspecifically bound and free radioligand, and C_S [Bq cm^{-3}] is the radioactivity concentration of the radioligand specifically bound to receptors. C_T [Bq cm^{-3}] is the radioactivity concentration in a brain region measured by PET or SPECT.

Note that the arterial input function C_P is just the unchanged radioligand in plasma. The free fraction of radioligand in plasma is the fraction of the ligand that is not bound to plasma proteins at equilibrium. The plasma free fraction is referred to as f_P, and the concentration of free exchangeable radioligand in plasma C_{FP} can be calculated as:

$$C_{FP}(t) = f_P C_P(t) \tag{11.6}$$

Actually, for simplicity, unchanged plasma radioactivity concentration (C_P) is used for neuroreceptor modeling. Brain tissues usually have a small fraction of volume occupied by blood (~5%) and Eq. 11.5 may be re-written as:

$$C_T(t) = (1 - V_B)\left[C_{ND}(t) + C_S(t)\right] + V_B C_a(t) \tag{11.7}$$

where V_B is the fraction of the measured volume occupied by blood. Because the multiplication of blood volumes and radioactivity in whole blood C_a in the human brain are small (Kuhl et al. 1975), the blood volume term is often omitted.

11.3.3 Relation Between the Concept of Receptor Binding and Kinetic Model

The pharmacological parameters described above (e.g. B_{max}, BP) can be linked to the kinetic model parameters. As the unlabeled "cold" ligand is present during the preparation of many radioligands that will compete at binding sites with the labeled tracer, the proportion of labeled tracer to the total amount of injected ligand (specific activity, SA [GBq·μmol^{-1}]) must also be considered in the equations:

$$\begin{aligned} k_3 &= k'_{on} f_{ND} \left(B_{avail} - C_S / SA \right) \\ k_4 &= k'_{off} \end{aligned} \tag{11.8}$$

where k'_{on} [L^{-1}·nmol·min^{-1}] and k'_{off} [L^{-1}·nmol·min^{-1}] are biomolecular association and dissociation rate constants. f_{ND} is the free fraction of radioligand in non-displaceable compartment, B_{avail} [L^{-1}·nmol] is receptor density available to bind radioligand *in vivo*, where B_{avail} can be regarded as (B_{max} – B_{occup}) (B_{occup}: number of receptors occupied by the endogenous ligand). If the amount of total receptor-binding ligand C_S/SA is very small relative to the binding capacity (B_{avail}), it can be disregarded and k_3 is then equal to the first term, i.e. $k'_{on} f_{ND} B_{avail}$.

$$\frac{k_3}{k_4} = f_{ND} \frac{B_{avail}}{K_D} \tag{11.9}$$

Here $K_D = k'_{off}/k'_{on}$. Finally, the binding potential relative to the radioactivity concentration of non-displaceable radioligand in the brain (BP_{ND}), which reflects the ratio of available receptor density (B_{avail}) and affinity (K_D) is defined as follows:

$$BP_{ND} = \frac{k_3}{k_4} \tag{11.10}$$

Full kinetic fits to determine receptor density (B_{avail}) and affinity of radioligand (K_D) are usually obtained from multiple PET/SPECT scans with various SA of radioligands (Delforge et al. 1989; Farde et al. 1989; Gallezot et al. 2008). There has been growing interest in detecting multiple functions simultaneously with single PET/SPECT data acquisition using multiple tracer injections (Ikoma et al. 2009; Koeppe et al. 2001). However, these approaches are still complicated for routine use. Alternatively, it is useful to employ a combination of parameters like BP_{ND} (instead of B_{avail}, K_D, k_3 and k_4) as a macro-parameter to represent the observed data

rather than considering the individual parameters. The distribution volume is one of the macro-parameters and the basic concept originated from volume of distribution in pharmacokinetics, which connects the administered dose to the actual initial concentration present in the circulation at the equilibrium. This concept was adopted in the field of *in vivo* imaging. Instead of referring to total administrated dose in the entire body, the distribution volume (V_T) is expressed as the activity of radioligand in the tissue as follows:

$$V_T = \frac{C_T}{C_p} = V_{ND} + V_S = \frac{C_{ND}}{C_p} + \frac{C_S}{C_p} \tag{11.11}$$

where C_{ND} and C_S are the radioactivity concentrations in non-displaceable and specific bound in the tissue, respectively. An important assumption is that the radioactive concentration in V_T must satisfy the equilibrium condition. However, it is difficult to achieve complete secular equilibrium practically where "the rate of change of the concentration in the compartment is zero" due to the limited imaging time (e.g. 1–2 h), physical half-life of isotopes, and other biological reasons. In the case of exchange between compartments in neuroreceptor studies, the term "transient equilibrium", where the maximum turning point of radioactivity concentration, is used (Farde et al. 1989; Ito et al. 1998a). Although at this point the change of concentration is zero, there may still be exchange between compartments (e.g. tissue and blood) and the total loss from the system is not negligible.

An important concept of pharmacokinetics is that the ratio of compartmental rate constant equals selected equilibrium distribution volumes. If C_{ND} and C_S simultaneously reach equilibrium, differentiations in Eq. 11.5, dC_{ND}/dt and dC_S/dt, become zero. After arrangement of Eq. 11.5 with equilibrium conditions, the distribution volumes as expression of rate constant are as follows:

$$\begin{aligned} V_{ND} &= \frac{K_1}{k_2} \\ V_S &= \frac{K_1}{k_2} \cdot \frac{k_3}{k_4} \\ V_T &= V_{ND} + V_S = \frac{K_1}{k_2} \cdot \left(1 + \frac{k_3}{k_4}\right) \end{aligned} \tag{11.12}$$

BP_{ND} are also expressed by the ratio of distribution volumes as follows:

$$BP_{ND} = \frac{k_3}{k_4} = \frac{V_S}{V_{ND}} = \frac{\left(V_T - V_{ND}\right)}{V_{ND}} \tag{11.13}$$

11.4 Quantification of Receptor Imaging Studies

11.4.1 General Considerations

In standard neuroreceptor compartmental models (Fig. 11.4), the total radioactivity concentration C_T is mathematically expressed as a summation of two compartments as follows:

$$C_T(t) = \frac{K_1}{\alpha_1 - \alpha_2}\left\{(\alpha_1 - k_3 - k_4)e^{-\alpha_1 t} - (\alpha_2 - k_3 - k_4)e^{-\alpha_2 t}\right\} \otimes C_p(t)$$
$$\alpha_{1,2} = \frac{k_2 + k_3 + k_4 \pm \sqrt{(k_2 + k_3 + k_4)^2 - 4k_2k_4}}{2} \tag{11.14}$$

For estimation of the K parameters from this nonlinear equation, an iterative nonlinear fitting procedure with an arterial input function (C_p) is necessary. Quantification of the labeled radioligand in the plasma requires to obtain plasma radioactivity concentration, time-course of arterial blood sampling, and plasma separation. Instead of this burden, the large number of parameters introduces instability and variability in the estimates in addition to lengthy calculation time. Therefore, usually the outcome measure in *in vivo* neuroreceptor imaging is BP_{ND} or V_T as macro-parameters rather than k-parameters themselves. Sometimes one of alternative estimation processes, namely "graphical analysis", is used. This graphical analysis is very useful because of rapid calculation and stability in the estimates.

Furthermore, arterial sampling is invasive and technically demanding. If the heart chamber is scanned and imaged simultaneously with the brain, the arterial input function can be directly derived from dynamic images (Iida et al. 1998; Watabe et al. 2005). Alternatively, the input function can be extracted as a component through image processing of dynamic images (Naganawa et al. 2005; Wu et al. 1995). In some applications for receptor studies, the arterial input function can be replaced by a reference to tissue devoid of specific binding sites. A typical derivation of the non-invasive reference technique is the "simplified reference tissue model" (Lammertsma and Hume 1996). Although this approach has several advantages such as non-invasiveness over the method requiring an arterial input function, several assumptions are associated with the simplified technique and as such caution is mandatory for its use.

As a different solution to Eq. 11.5, the experimental paradigm starts with bolus injection of the radiotracer followed by continuous infused administration of the radiotracer to achieve constant concentrations in the tissue and blood (Carson et al. 1993). In this protocol, V_T and BP_{ND} can be easily obtained by calculating ratios between the radioactivity concentration in tissue and blood. The rate of infusion may vary between subjects, and optimal scheduling of the experiments must be sought for the success of the bolus plus infusion paradigm.

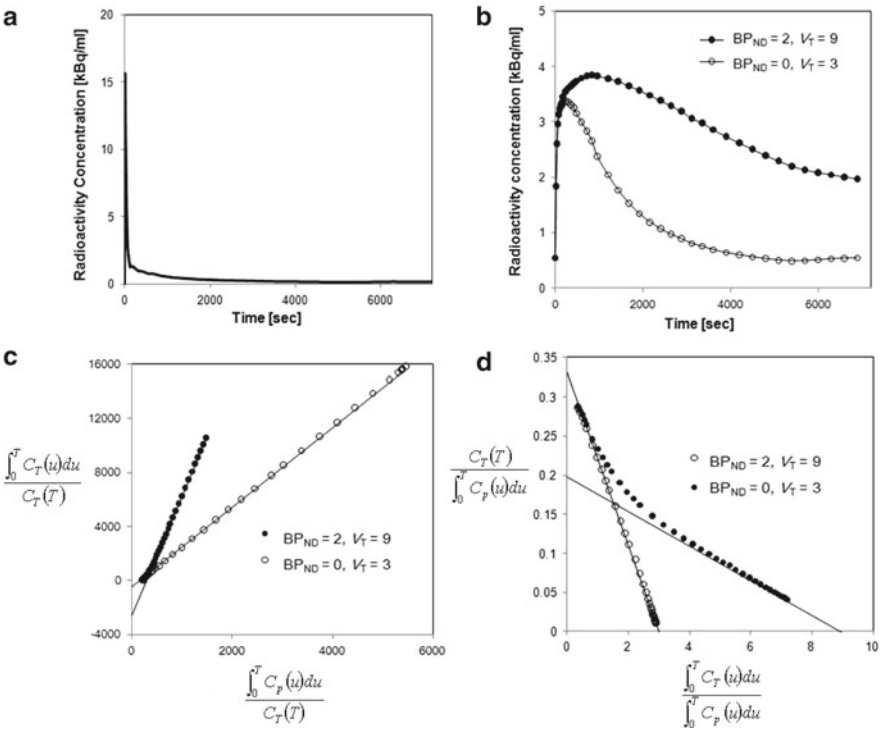

Fig. 11.5 Illustration of time-activity curves and the graphical analysis; (**a**) time-activity curve of plasma input function (C_p) and (**b**) time-activity curves of tissue (C_T) with $K_1=0.33$, $k_2=0.11$, $k_3=0.08$, $k_4=0.04$ ($V_T=9$, $BP_{ND}=2$) and with $K_1=0.33$, $k_2=0.11$ ($V_T=3$, $BP_{ND}=0$). Two tissue curves are graphically plotted with (**c**) Logan graphical analysis and (**d**) Ito-Yokoi plot

11.4.2 Graphical Analysis

The graphical analysis generally allows quick estimation by graphically fitting a straight line to experimental data or using linear regression analysis. Since it is often difficult to achieve equilibrium conditions, an approximation is used from a graphic representation of kinetic data.

Logan graphical analysis was originally proposed to quantify the total volume of distribution, V_T, for reversibly binding neuroreceptor tracers (Logan et al. 1990). V_T is equivalent to the slope only after reaching equilibrium where the relationship between the two terms of the ratio: the integrated arterial plasma input function (C_p) and the radioactivity concentration in tissue (C_T) becomes linear (Fig. 11.5c). The advantages of using Logan graphical analysis are the rapid determination of V_T and its low variance. V_T is estimated from the following equation:

$$\frac{\int_0^t C_T(u)du}{C_T(t)} = V_T \frac{\int_0^t C_p(u)du}{C_T(t)} + b \qquad t \geq t^*, \tag{11.15}$$

Because V_T and b become constant only after equilibrium time for regression t^*, they are estimated as a slope and an intercept, respectively, using the frames of $t \geq t^*$. The equilibrium time (t^*) for linear regression is different from equilibrium in compartmental models; however, there are still two drawbacks, noise-induced bias in the estimates and objective determination of t^* (Slifstein and Laruelle 2000).

Another approach consists in rearranging Eq. 11.15 into multi-linear form to give Eq. 11.16 (Ichise et al. 2002). This approach is usually called multilinear analysis (MA1).

$$C_T(t) = \beta_1 \int_0^t C_p(u)du + \beta_2 \int_0^t C_T(u)du \qquad t \geq t^* \tag{11.16}$$

$\beta_1 = -V_T/b$ and $\beta_2 = 1/b$ are estimated by linear regression analysis for $t \geq t^*$, and V_T is calculated as $-\beta_1/\beta_2$. Furthermore, Ichise et al. proposed several rigorous approaches, e.g. multilinear analysis (MA2) which does not require t^* (Ichise et al. 2001, 2002, 2003).

Even though both Logan graphical analysis and multilinear analysis provide only estimates for V_T, as a recent progressive work, Ito and Yokoi proposed an alternative graphical analysis for neuroreceptor imaging, which can be used to calculate both V_T and V_{ND} (Ito et al. 2010). In other words, BP_{ND} (= $V_T/V_{ND} - 1$) can also be estimated as a result. This approach assumes that the time-activity curve is also described by the one-tissue compartment model with two rate constants (Ito et al. 1996; Koeppe et al. 1991). The rate constants, K_i and k_o are the influx and efflux rate constants for the radioligand diffusion through the BBB, respectively, and V_T is defined as K_i/k_o. After integration and arrangement of differential equations based on the two-tissue compartment model given by Eq. 11.5 and the one-tissue compartment model with K_i and k_o, the graphical equilibrium at $t \to 0$ and $t \geq t^*$ will be expressed as follows:

$$Y(t) = \begin{cases} K_1 - k_2 X(t) & t \to 0 \\ K_i - k_o X(t) & t \geq t^* \end{cases}$$

$$X(t) = \frac{\int_0^t C_T(u)du}{\int_0^t C_p(u)du}, \qquad Y(t) = \frac{C_T(u)}{\int_0^t C_p(u)du} \tag{11.17}$$

From Eq. 11.17, both x and y intercepts at each condition ($t \to 0$ and $t \geq t^*$) become as follows:

$$x - \text{int}\,ercept = \begin{cases} V_{ND} = \dfrac{K_1}{k_2} & t \to 0 \\ V_T = \dfrac{k_i}{k_o} & t \geq t^* \end{cases}$$

$$y - \text{int}\,ercept = \begin{cases} K_1 & t \to 0 \\ K_i & t \geq t^* \end{cases} \tag{11.18}$$

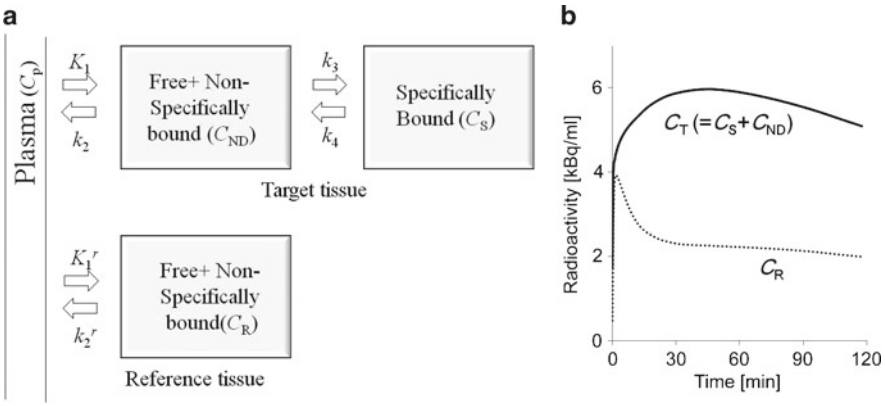

Fig. 11.6 Standard reference tissue model for receptor-binding radioligands (**a**) and time courses of radioactivity in the two compartments C_T and C_R (**b**)

An example plot of this approach is shown in Fig. 11.5d. Advantages of this method can be used to know whether the radioligand binding includes specific binding or not according to the shape of the plot (Ito et al. 2010).

11.4.3 Reference Approach

11.4.3.1 Reference Tissue Region

For most radioligands, reference region with low specific binding can be used as indirect input function to the region containing the specific receptors of interest. A compartment model incorporating the reference region is illustrated in Fig. 11.6 (Blomqvist et al. 1989; Cunningham et al. 1991). Because of low specific binding, radioactivity concentration in the reference region (C_R) is expressed as influx/efflux between only plasma and reference tissue with rate constants K_1^r [mL·cm^{-3}·min^{-1}] and k_2^r [min^{-1}].

$$\frac{dC_R(t)}{dt} = K_1^r \cdot C_p(t) - k_2^r \cdot C_R(t) \tag{11.19}$$

The transient equilibrium that theoretically occurs when the derivative for specific binding ($dC_S(t)/dt$) is 0, that is, the peak point of specific binding, $C_S(t)$, is a simple method for BP_{ND} estimation using reference tissue (Ito et al. 1998a). It follows that $C_S(t)/C_{ND}(t)$ is equal to k_3/k_4 (=BP_{ND}) at transient equilibrium (here $C_{ND} \approx C_R$). However, the existence of specific binding in the reference region directly influence the estimates of BP_{ND} though this transient equilibrium method.

11.4.3.2 Simplified Reference Tissue Model (SRTM)

The SRTM yields the binding potential value by eliminating the arterial input function, C_p, arithmetically from model equations by using a TAC from a reference region where specific bindings are negligible, under the assumptions that the distribution volume of the non-displaceable compartment in the target and reference regions are equal, and that a target region can be described with the one-tissue compartment model given by Eq. 11.20.

$$C_T(t) = R_1 \cdot C_R(t) + \left(k_2 - \frac{R_1 k_2}{1 + BP_{ND}} \right) \cdot e^{\left(-\frac{k_2}{1+BP_{ND}} t \right)} \otimes C_R(t)$$
$$R_1 = K_1 / K_1^r \tag{11.20}$$

where C_T and C_R are the radioactivity concentrations in the target and reference regions, respectively. SRTM estimates three parameters, the delivery ratio of the target region to the reference region (R_1), the clearance rate constant of the target region (k_2), and binding potential, referred to as BP_{ND} by non-linear least squares analysis.

11.4.3.3 Noninvasive Graphical Analysis

As a noninvasive Logan plot distribution volume ratio DVR can be estimated as follows (Logan et al. 2001):

$$\frac{\int_0^t C_T(u)du}{C_T(t)} = DVR \left(\frac{\int_0^t C_R(u)du}{C_T(t)} + \frac{C_R(t)/k_2^r}{C_T(t)} \right) + b \qquad t \geq t^*, \tag{11.21}$$

where DVR is defined as the ratio of V_T in the target and reference regions and BP_{ND} is expressed as (DVR − 1). k_2^r is the efflux rate constant k_2 in the reference region. Equation 11.20 can also be extended as a multi-linear formulation. However, determination of k_2^r still remains to be done (Ichise et al. 2003). By using a more strict assumption that C_R is proportional to C_p after equilibrium, Zhou et al. have recently proposed simplified noninvasive graphical plot with reference tissue region (Zhou et al. 2010).

$$\frac{\int_0^t C_T(u)du}{C_R(t)} = DVR \frac{\int_0^t C_R(u)du}{C_R(t)} + b \qquad t \geq t^* \tag{11.22}$$

Even though the assumption of this approach is strict, it is not necessary to define k_2^r in advance and the robustness for noise-induced bias provides stable estimates and this is effective in the case of parametric imaging through pixel-by-pixel estimation process.

11.4.4 Parametric Imaging

In practice, PET measurement $C_T(t)$ has two derivations, at region of interest (ROI) and voxel levels. Parametric imaging indicates voxel-by-voxel estimation of $C(t)$ (Rahmim et al. 2009; Tsoumpas et al. 2008). Due to limited statistical count and temporal resolution of PET and SPECT, noise properties of $C_T(t)$ at the voxel level is poor. Therefore, when parametric imaging is used, the effect of noise on the estimate must be carefully considered. In essence, the effect of noise appears as a noise-induced bias and variance of the estimates and these amounts depend on the kind of analysis used (Ikoma et al. 2008). Furthermore, the number of pixels in the PET image is very large. The computing time for deriving $C_T(t)$ for each pixel is also one of the issues that need to be considered. In other words, time consuming approaches such as non-linear least square fitting, are not desirable for parametric imaging.

Noise-induced bias of V_T in Logan graphical analysis is well-known issue, especially in parametric imaging (Slifstein and Laruelle 2000). The simplified approach derived by Zhou et al. enables stable estimation because the denominator in the graphical analysis has relatively good statistics (i.e. using $C_R(t)$ instead of $C_T(t)$) (Zhou et al. 2010). In order to fasten computing time and improve the stability of the estimates, the SRTM method can be extended using basis function approach (Gunn et al. 1997). As a direct solution, suppressing noise in $C_T(t)$ at each pixel has been investigated (Joshi et al. 2008; Shidahara et al. 2007; Turkheimer et al. 2000). Recent advances in 4D-reconstruction resulting in the generation of parametric images may be a potent approach (Rahmim et al. 2009; Tsoumpas et al. 2008).

11.5 Clinical and Research Applications of Receptor Imaging

11.5.1 Neurodegenerative Disease (e.g. Dopaminergic Function in Parkinson Disease)

Idiopathic Parkinson's disease (IPD) is the most prevalent neurodegenerative disease after dementia, with an estimated prevalence of 150 per 100,000 and incidence of 20 per 100,000. The typical clinical symptoms such as rigidity, hypokinesia, tremor and postural instability, are associated to the degeneration of dopaminergic neurons in the substantia nigra of the brainstem. Although IPD is the most prevalent cause of Parkinsonism, there are other diseases that present with one or more similar symptoms (Van Laere and Zaidi 2006). Recent studies have demonstrated that of the patients that deceased under the diagnosis IPD, up to 25% actually did not have the disease (Lang and Lozano 1998). Various radioligands are currently commercially available to evaluate the pre- and postsynaptic status of the dopaminergic system (Booij et al. 1999). Both ^{123}I labelled iodobenzamide (IBZM) and epidepride, as well as ^{11}C-raclopride can be used as a sensitive differentiator between IPD and other Parkinsonian syndromes, and are predictive for the response on dopaminergic therapy (Schwarz et al. 1997). In Parkinson's disease, the postsynaptic system is

normal to upregulated, while in the most Parkinsonian syndromes, of which multi system atrophy (MSA) and progressive supranuclear palsy (PSP) are the most common, there is a decreased postsynaptic binding. The cocaine-analogue ^{123}I-FP-CIT (ioflupane) has a clinical role in the early diagnosis of Parkinson's disease (since abnormalities are present even 5 years before clinical symptomatology), differentiation between IPD and essential tremor, as well as in the differentiation between Alzheimer and Lewy body dementia (Costa et al. 1999). This tracer is very sensitive for presynaptic damage to the striatum and the uptake in the contralateral striatum is correlated to the severity of clinical disease (Seibyl et al. 1995).

Despite controversial clinico-pathological distinctions between Parkinson's disease with dementia (PDD) and DAT, similar patterns of metabolic reduction in the posterior brain were reported previously using PET with ^{18}F-FDG. More specific regional differences were measured between PDD and DAT using accurate and objective brain mapping techniques. PDD showed greater metabolic reduction in the visual cortex and relatively preserved metabolism in the medial temporal cortex (Vander et al. 1997).

Metabolic or perfusion brain imaging is useful in the differential diagnosis of extrapyramidal disorders due to the application of anatomical standardization (Bosman et al. 2003; Spetsieris et al. 1995). Progressive supranuclear palsy (PSP) and corticobasal degeneration (CBD) are neurodegenerative disorders that may be accompanied by dementia and Parkinsonism as clinical symptoms. Measurement of glucose metabolism by PET and a voxel-based analysis is useful to understand the pathophysiology and differentiate IPD and corticobasal degeneration with cognitive impairments (Hosaka et al. 2002).

11.5.2 Receptor Occupancy (e.g. Antipsychotic-Drug Evaluation)

Explicit labeling of striatal receptors with radioligands has been used to determine receptor occupancy during treatment with antipsychotic drugs. The most prevalent application of neuroreceptor imaging in schizophrenia during the last two decades has been the evaluation of receptor occupancy accomplished by antipsychotic drugs. The major spotlight has been on D_2 receptor occupancy although $5HT_{2A}$ and D_1 receptors have also been considered (Laruelle et al. 2003). Several studies have reported the existence of a threshold of occupancy of striatal D_2 receptors beyond which extrapiramidal side effects (EPS) are likely to take place. It has been difficult to establish a relationship between the degree of D_2 receptor occupancy and clinical response. It should be noted that most studies have been carried out at doses reaching more than 50% occupancy and the minimum occupancy needed for observing a therapeutic response still needs to be defined. It has, however, been demonstrated that in few studies carried out with relatively low doses of D_2 receptor antagonists that 50–60% occupancy is needed to monitor a prompt clinical response (Laruelle et al. 2003). It has been determined that antipsychotic action requires a receptor occupancy of 60%, although extrapyramidal side effects occur at ≥80% receptor occupancy (Heiss and Herholz 2006).

Although currently the clinical indications for receptor imaging are limited to predominantly movement disorders, they do show potential for clinical dose titration of medication, early diagnosis of neuropsychiatry disorders, as well as more specific localization of cerebral functional disturbances. Many other applications have been reported in the literature but fall beyond the scope of this review (Heiss and Herholz 2006; Laruelle et al. 2003).

11.6 Summary and Future Perspectives

During the last two decades, molecular neuroreceptor imaging using SPECT and PET has advanced elegantly and steadily gained importance in the clinical and research arenas. High resolution cutting-edge SPECT and PET neuroimaging is poised to advance our understanding of the pathophysiological mechanisms of neurological and psychiatric diseases and in the clinical management of patients. Software- and hardware-based multimodality brain imaging (e.g. PET/MR) has enabled the implementation of sophisticated anatomical-guided quantitative PET procedures that will undoubtedly revolutionize clinical diagnosis and offer unique capabilities for the clinical neuroreceptor imaging community and neuroscience researchers at large.

Frontiers of molecular neuroreceptor imaging research are also being expanded with small-animal brain imaging using dedicated high-resolution SPECT and PET instrumentation in addition to optical imaging and high-field MR imaging (Stout and Zaidi 2008). Most preclinical imaging systems require animals to remain motionless for several minutes to hours in order to obtain useful data, thus some type of anesthesia is necessary. There is considerable interest in imaging without anesthesia, since conscious animals have normal physiological functions compared to those under anesthesia. Several groups have shown that this is indeed feasible under some circumstances (Ferris et al. 2006; Kyme et al. 2008). These observations spurred the development of the rat conscious animal PET scanner (RatCAP), a complete 3D PET scanner designed to image the brain of an awake rat (Vaska et al. 2004), that incorporates the PET system into an integrated, compact arrangement of detector arrays with highly integrated electronics (Woody et al. 2007). Nonetheless, most preclinical neuroreceptor imaging research at present is conducted using anesthesia, and the type and injection route can play a significant role in the sedation and physiological status of the animal. It is expected that the triad molecular neuroscience, genetics and imaging will expand the understanding of the pathophysiology within the psychiatric and neurological clinical diseases in the coming decennia, hopefully leading to improved diagnosis and treatment, and eventually to the implementation of preventive techniques.

Acknowledgements This work was supported by the Swiss National Science Foundation under grants SNSF 31003A-135576 and SNSF 33CM30-124114.

References

Accorsi R (2008) Brain single-photon emission CT physics principles. AJNR Am J Neuroradiol 29:1247–1256

Agdeppa ED, Kepe V, Liu J, Small GW, Huang SC, Petric A, Satyamurthy N, Barrio JR (2003) 2-Dialkylamino-6-acylmalononitrile substituted naphthalenes (DDNP analogs): novel diagnostic and therapeutic tools in Alzheimer's disease. Mol Imaging Biol 5:404–417

Bentourkia M, Zaidi H (2007) Tracer kinetic modeling in PET. PET Clinics 2:267–277

Blomqvist G, Pauli S, Farde L, Eriksson L, Person A, Halldin C (1989) Dynamic models for reversible ligand binding. Kluwer, Dordrecht

Booij J, Tissingh G, Winogrodzka A, van Royen EA (1999) Imaging of the dopaminergic neurotransmission system using single- photon emission tomography and positron emission tomography in patients with Parkinsonism. Eur J Nucl Med 26:171–182

Bosman T, Van Laere K, Santens P (2003) Anatomically standardised (99 m)Tc-ECD brain perfusion SPET allows accurate differentiation between healthy volunteers, multiple system atrophy and idiopathic Parkinson's disease. Eur J Nucl Med Mol Imaging 30:16–24

Brucke T, Kornhuber J, Angelberger P, Asenbaum S, Frassine H, Podreka I (1993) SPECT imaging of dopamine and serotonin transporters with [123I]beta-CIT. Binding kinetics in the human brain. J Neural Transm Gen Sect 94:137–146

Burns HD, Dannals RF, Langstrom B, Ravert HT, Zemyan SE, Duelfer T, Wong DF, Frost JJ, Kuhar MJ, Wagner HN (1984) (3-N-[11C]methyl)spiperone, a ligand binding to dopamine receptors: radiochemical synthesis and biodistribution studies in mice. J Nucl Med 25:1222–1227

Carson RE, Channing MA, Blasberg RG, Dunn BB, Cohen RM, Rice KC, Herscovitch P (1993) Comparison of bolus and infusion methods for receptor quantitation: application to [18F] cyclofoxy and positron emission tomography. J Cereb Blood Flow Metab 13:24–42

Cho ZH, Son YD, Kim HK, Kim KN, Oh SH, Han JY, Hong IK, Kim YB (2008) A fusion PET-MRI system with a high-resolution research tomograph-PET and ultra-high field 7.0 T-MRI for the molecular-genetic imaging of the brain. Proteomics 8:1302–1323

Costa D, Walker Z, Walker R et al (1999) Dementia with Lewy bodies: preliminary data on clinical, pathological and FP-CIT SPECT correlations. Nucl Med Comm 20:467–468

Crouzel C, Guillaume M, Barre L, Lemaire C, Pike VW (1992) Ligands and tracers for PET studies of the 5-HT system–current status. Int J Rad Appl Instrum B 19:857–870

Cunningham VJ, Hume SP, Price GR, Ahier RG, Cremer JE, Jones AK (1991) Compartmental analysis of diprenorphine binding to opiate receptors in the rat in vivo and its comparison with equilibrium data in vitro. J Cereb Blood Flow Metab 11:1–9

Delforge J, Syrota A, Mazoyer BM (1989) Experimental design optimization: theory and application to estimation of receptor model parameters using dynamic positron emission tomography. Phys Med Biol 34:419–435

Dresel S, Kung MP, Huang XF, Plossl K, Hou C, Meegalla SK, Patselas GP, Mu M, Saffer JR, Kung HK (1999) Simultaneous SPECT studies of pre- and postsynaptic dopamine binding sites in baboons. J Nucl Med 40:660–666

Emond P, Garreau L, Chalon S, Boazi M, Caillet M, Bricard J, Frangin Y, Mauclaire L, Besnard JC, Guilloteau D (1997) Synthesis and ligand binding of nortropane derivatives: N-substituted 2beta-carbomethoxy-3beta-(4′-iodophenyl)nortropane and N-(3-iodoprop-(2E)-enyl)-2beta-carbomethoxy-3beta-(3′,4′-disubstituted phenyl)nortropane. New high-affinity and selective compounds for the dopamine transporter. J Med Chem 40:1366–1372

Farde L, Halldin C, Stone-Elander S, Sedvall G (1987) PET analysis of human dopamine receptor subtypes using 11C-SCH 23390 and 11C-raclopride. Psychopharmacology (Berl) 92:278–284

Farde L, Eriksson L, Blomqvist G, Halldin C (1989) Kinetic analysis of central [11C]Raclopride binding to D2-dopamine receptors studied by PET – a comparison to the equilibrium analysis. J Cereb Blood Flow Metab 9:696–708

Farde L, Halldin C, Muller L, Suhara T, Karlsson P, Hall H (1994) PET study of [11C]beta-CIT binding to monoamine transporters in the monkey and human brain. Synapse 16:93–103
Ferris CF, Febo M, Luo F, Schmidt K, Brevard M, Harder JA, Kulkarni P, Messenger T, King JA (2006) Functional magnetic resonance imaging in conscious animals: a new tool in behavioural neuroscience research. J Neuroendocrinol 18:307–318
Fowler JS, Volkow ND, Wang GJ, Ding YS (2004) 2-deoxy-2-[18F]fluoro-D-glucose and alternative radiotracers for positron emission tomography imaging using the human brain as a model. Semin Nucl Med 34:112–121
Furumoto S, Okamura N, Iwata R, Yanai K, Arai H, Kudo Y (2007) Recent advances in the development of amyloid imaging agents. Curr Top Med Chem 7:1773–1789
Gallezot JD, Bottlaender MA, Delforge J, Valette H, Saba W, Dolle F, Coulon CM, Ottaviani MP, Hinnen F, Syrota A, Gregoire MC (2008) Quantification of cerebral nicotinic acetylcholine receptors by PET using 2-[18F]fluoro-A-85380 and the multiinjection approach. J Cereb Blood Flow Metab 28:172–180
Gilman S (1998) Imaging the brain. First of two parts. N Engl J Med 338:812–820
Gunn RN, Lammertsma AA, Hume SP, Cunningham VJ (1997) Parametric imaging of ligand-receptor binding in PET using a simplified reference region model. Neuroimage 6:279–287
Halldin C, Stone-Elander S, Farde L, Ehrin E, Fasth KJ, Langstrom B, Sedvall G (1986) Preparation of 11C-labelled SCH 23390 for the in vivo study of dopamine D-1 receptors using positron emission tomography. Int J Rad Appl Instrum A 37:1039–1043
Halldin C, Foged C, Chou YH, Karlsson P, Swahn CG, Sandell J, Sedvall G, Farde L (1998) Carbon-11-NNC 112: a radioligand for PET examination of striatal and neocortical D1-dopamine receptors. J Nucl Med 39:2061–2068
Halldin C, Gulyas B, Langer O, Farde L (2001) Brain radioligands–state of the art and new trends. Q J Nucl Med 45:139–152
Hammoud DA, Hoffman JM, Pomper MG (2007) Molecular neuroimaging: from conventional to emerging techniques. Radiology 245:21–42
Hartvig P, Agren H, Reibring L, Tedroff J, Bjurling P, Kihlberg T, Langstrom B (1991) Brain kinetics of L-[beta-11C]dopa in humans studied by positron emission tomography. J Neural Transm Gen Sect 86:25–41
Heiss WD, Herholz K (2006) Brain receptor imaging. J Nucl Med 47:302–312
Hosaka K, Ishii K, Sakamoto S, Mori T, Sasaki M, Hirono N, Mori E (2002) Voxel-based comparison of regional cerebral glucose metabolism between PSP and corticobasal degeneration. J Neurol Sci 199:67–71
Houle S, DaSilva JN, Wilson AA (2000) Imaging the 5-HT(1A) receptors with PET: WAY-100635 and analogues. Nucl Med Biol 27:463–466
Ichise M, Meyer JH, Yonekura Y (2001) An introduction to PET and SPECT neuroreceptor quantification models. J Nucl Med 42:755–763
Ichise M, Toyama H, Innis RB, Carson RE (2002) Strategies to improve neuroreceptor parameter estimation by linear regression analysis. J Cereb Blood Flow Metab 22:1271–1281
Ichise M, Liow JS, Lu JQ, Takano A, Model K, Toyama H, Suhara T, Suzuki K, Innis RB, Carson RE (2003) Linearized reference tissue parametric imaging methods: application to [11C]DASB positron emission tomography studies of the serotonin transporter in human brain. J Cereb Blood Flow Metab 23:1096–1112
Iida H, Miura S, Shoji Y, Ogawa T, Kado H, Narita Y, Hatazawa J, Eberl S, Kanno I, Uemura K (1998) Noninvasive quantitation of cerebral blood flow using oxygen-15-water and a dual-PET system. J Nucl Med 39:1789–1798
Ikoma Y, Watabe H, Shidahara M, Naganawa M, Kimura Y (2008) PET kinetic analysis: error consideration of quantitative analysis in dynamic studies. Ann Nucl Med 22:1–11
Ikoma Y, Watabe H, Hayashi T, Miyake Y, Teramoto N, Minato K, Iida H (2009) Quantitative evaluation of changes in binding potential with a simplified reference tissue model and multiple injections of [11C]raclopride. Neuroimage 47:1639–1648
Innis RB, Cunningham VJ, Delforge J, Fujita M, Gjedde A, Gunn RN, Holden J, Houle S, Huang SC, Ichise M, Iida H, Ito H, Kimura Y, Koeppe RA, Knudsen GM, Knuuti J, Lammertsma AA, Laruelle M, Logan J, Maguire RP, Mintun MA, Morris ED, Parsey R, Price JC, Slifstein M,

Sossi V, Suhara T, Votaw JR, Wong DF, Carson RE (2007) Consensus nomenclature for in vivo imaging of reversibly binding radioligands. J Cereb Blood Flow Metab 27:1533–1539

Ito H, Goto R, Koyama M, Kawashima R, Ono S, Sato K, Fukuda H (1996) A simple method for the quantification of benzodiazepine receptors using iodine-123 iomazenil and single-photon emission tomography. Eur J Nucl Med 23:782–791

Ito H, Hietala J, Blomqvist G, Halldin C, Farde L (1998a) Comparison of the transient equilibrium and continuous infusion method for quantitative PET analysis of [11C]raclopride binding. J Cereb Blood Flow Metab 18:941–950

Ito H, Nyberg S, Halldin C, Lundkvist C, Farde L (1998b) PET imaging of central 5-HT2A receptors with carbon-11-MDL 100,907. J Nucl Med 39:208–214

Ito H, Takahashi H, Arakawa R, Takano H, Suhara T (2008) Normal database of dopaminergic neurotransmission system in human brain measured by positron emission tomography. Neuroimage 39:555–565

Ito H, Yokoi T, Ikoma Y, Shidahara M, Seki C, Naganawa M, Takahashi H, Takano H, Kimura Y, Ichise M, Suhara T (2010) A new graphic plot analysis for determination of neuroreceptor binding in positron emission tomography studies. Neuroimage 49:578–586

Jacobs AH, Li H, Winkeler A, Hilker R, Knoess C, Ruger A, Galldiks N, Schaller B, Sobesky J, Kracht L, Monfared P, Klein M, Vollmar S, Bauer B, Wagner R, Graf R, Wienhard K, Herholz K, Heiss WD (2003) PET-based molecular imaging in neuroscience. Eur J Nucl Med Mol Imaging 30:1051–1065

Joshi A, Fessler JA, Koeppe RA (2008) Improving PET receptor binding estimates from Logan plots using principal component analysis. J Cereb Blood Flow Metab 28:852–865

Klunk WE, Engler H, Nordberg A, Wang Y, Blomqvist G, Holt DP, Bergstrom M, Savitcheva I, Huang GF, Estrada S, Ausen B, Debnath ML, Barletta J, Price JC, Sandell J, Lopresti BJ, Wall A, Koivisto P, Antoni G, Mathis CA, Langstrom B (2004) Imaging brain amyloid in Alzheimer's disease with Pittsburgh Compound-B. Ann Neurol 55:306–319

Koeppe RA, Holthoff VA, Frey KA, Kilbourn MR, Kuhl DE (1991) Compartmental analysis of [11C]flumazenil kinetics for the estimation of ligand transport rate and receptor distribution using positron emission tomography. J Cereb Blood Flow Metab 11:735–744

Koeppe RA, Raffel DM, Snyder SE, Ficaro EP, Kilbourn MR, Kuhl DE (2001) Dual-[11C]tracer single-acquisition positron emission tomography studies. J Cereb Blood Flow Metab 21:1480–1492

Kudo Y, Okamura N, Furumoto S, Tashiro M, Furukawa K, Maruyama M, Itoh M, Iwata R, Yanai K, Arai H (2007) 2-(2-[2-Dimethylaminothiazol-5-yl]ethenyl)-6- (2-[fluoro]ethoxy)benzoxazole: a novel PET agent for in vivo detection of dense amyloid plaques in Alzheimer's disease patients. J Nucl Med 48:553–561

Kuhl DE, Reivich M, Alavi A, Nyary I, Staum MM (1975) Local cerebral blood volume determined by three-dimensional reconstruction of radionuclide scan data. Circ Res 36: 610–619

Kung HF, Kim HJ, Kung MP, Meegalla SK, Plossl K, Lee HK (1996) Imaging of dopamine transporters in humans with technetium-99 m TRODAT-1. Eur J Nucl Med 23:1527–1530

Kung MP, Hou C, Zhuang ZP, Zhang B, Skovronsky D, Trojanowski JQ, Lee VM, Kung HF (2002) IMPY: an improved thioflavin-T derivative for in vivo labeling of beta-amyloid plaques. Brain Res 956:202–210

Kyme AZ, Zhou VW, Meikle SR, Fulton RR (2008) Real-time 3D motion tracking for small animal brain PET. Phys Med Biol 53:2651–2666

Lammertsma AA, Hume SP (1996) Simplified reference tissue model for PET receptor studies. Neuroimage 4:153–158

Lang AE, Lozano AM (1998) Parkinson's disease. First of two parts. N Engl J Med 339:1044–1053

Laruelle M, Baldwin RM, Malison RT, Zea-Ponce Y, Zoghbi SS, al-Tikriti MS, Sybirska EH, Zimmermann RC, Wisniewski G, Neumeyer JL et al (1993) SPECT imaging of dopamine and serotonin transporters with [123I]beta-CIT: pharmacological characterization of brain uptake in nonhuman primates. Synapse 13:295–309

Laruelle M, Martinez D, Talbot P, Abi-Dargham A (2003) Molecular imaging in psychiatric disorders. In: Valk PE, Bailey DL, Townsend DW, Maisey MN (eds) Positron emission tomography: basic science and clinical practice. Springer, London, pp 399–426

Logan J, Fowler JS, Volkow ND, Wolf AP, Dewey SL, Schlyer DJ, MacGregor RR, Hitzemann R, Bendriem B, Gatley SJ et al (1990) Graphical analysis of reversible radioligand binding from time-activity measurements applied to [N-11C-methyl]-(−)-cocaine PET studies in human subjects. J Cereb Blood Flow Metab 10:740–747

Logan J, Fowler JS, Volkow ND, Ding YS, Wang GJ, Alexoff DL (2001) A strategy for removing the bias in the graphical analysis method. J Cereb Blood Flow Metab 21:307–320

Lundkvist C, Halldin C, Ginovart N, Nyberg S, Swahn CG, Carr AA, Brunner F, Farde L (1996) [11C]MDL 100907, a radioligland for selective imaging of 5-HT(2A) receptors with positron emission tomography. Life Sci 58:PL187–PL192

Michaelis L, Menten ML (1913) Die kinetic der Invertinwirkung. Biochemistry Zeitschrift 49:333–369

Muller L, Halldin C, Farde L, Karlsson P, Hall H, Swahn CG, Neumeyer J, Gao Y, Milius R (1993) [11C] beta-CIT, a cocaine analogue. Preparation, autoradiography and preliminary PET investigations. Nucl Med Biol 20:249–255

Naganawa M, Kimura Y, Ishii K, Oda K, Ishiwata K, Matani A (2005) Extraction of a plasma time-activity curve from dynamic brain PET images based on independent component analysis. IEEE Trans Biomed Eng 52:201–210

Oya S, Choi SR, Hou C, Mu M, Kung MP, Acton PD, Siciliano M, Kung HF (2000) 2-((2-((dimethylamino)methyl)phenyl)thio)-5-iodophenylamine (ADAM): an improved serotonin transporter ligand. Nucl Med Biol 27:249–254

Pike VW (2009) PET radiotracers: crossing the blood-brain barrier and surviving metabolism. Trends Pharmacol Sci 30:431–440

Pike VW, McCarron JA, Lammertsma AA, Osman S, Hume SP, Sargent PA, Bench CJ, Cliffe IA, Fletcher A, Grasby PM (1996) Exquisite delineation of 5-HT1A receptors in human brain with PET and [carbonyl-11C]WAY-100635. Eur J Pharmacol 301:R5–R7

Rahmim A, Zaidi H (2008) PET versus SPECT: strengths, limitations and challenges. Nucl Med Commun 29:193–207

Rahmim A, Tang J, Zaidi H (2009) Four-dimensional (4D) image reconstruction strategies in dynamic PET: beyond conventional independent frame reconstruction. Med Phys 36: 3654–3670

Rosso L, Gee AD, Gould IR (2008) Ab initio computational study of positron emission tomography ligands interacting with lipid molecule for the prediction of nonspecific binding. J Comput Chem 29:2397–2405

Scatchard G (1949) The attractions of proteins for small molecules and ions. Ann NY Acad Sci 51:660–672

Schlemmer HP, Pichler BJ, Schmand M, Burbar Z, Michel C, Ladebeck R, Jattke K, Townsend D, Nahmias C, Jacob PK, Heiss WD, Claussen CD (2008) Simultaneous MR/PET imaging of the human brain: feasibility study. Radiology 248:1028–1035

Schmidt KC and Turkheimer FE (2002) Kinetic modeling in positron emission tomography. Q J Nucl Med 46:70–85

Schwarz J, Tatsch K, Gasser T, Arnold G, Oertel WH (1997) [123]IBZM binding predicts dopaminergic responsiveness in patients with Parkinsonism and previous dopaminomimetic therapy. Mov Disord 12:898–902

Seibyl JP, Marek K, Quinlan D, Sheff K, Zoghbi S, Zea-Ponce Y, Baldwin RM, Fussell B, Smith EO, Charney DS (1995) Decreased 123Ibeta-CIT striatal uptake correlates with symptom severity in idiopathic Parkinson's disease. Ann Neurol 38:589–598

Shidahara M, Ikoma Y, Kershaw J, Kimura Y, Naganawa M, Watabe H (2007) PET kinetic analysis: wavelet denoising of dynamic PET data with application to parametric imaging. Ann Nucl Med 21:379–386

Shoghi-Jadid K, Small GW, Agdeppa ED, Kepe V, Ercoli LM, Siddarth P, Read S, Satyamurthy N, Petric A, Huang SC, Barrio JR (2002) Localization of neurofibrillary tangles and β-amyloid

plaques in the brains of living patients with Alzheimer disease. Am J Geriatr Psychiat 10:24–35
Slifstein M, Laruelle M (2000) Effects of statistical noise on graphic analysis of PET neuroreceptor studies. J Nucl Med 41:2083–2088
Sossi V (2007) Cutting-edge brain imaging with positron emission tomography. PET Clinics 2:91–104
Spetsieris PG, Moeller JR, Dhawan V, Ishikawa T, Eidelberg D (1995) Visualizing the evolution of abnormal metabolic networks in the brain using PET. Comput Med Imaging Graph 19:295–306
Stout DB, Zaidi H (2008) Preclinical multimodality imaging in vivo. PET Clin 3:251–273
Suehiro M, Scheffel U, Ravert HT, Dannals RF, Wagner HN Jr (1993) [11C](+)McN5652 as a radiotracer for imaging serotonin uptake sites with PET. Life Sci 53:883–892
Tikosfky RS, Ichise M, Seibyl JP, Verhoeff NPLG (1999) Functional brain SPECT imaging: 1999 and beyond. Semin Nucl Med 29:193–238
Tsoumpas C, Turkheimer FE, Thielemans K (2008) A survey of approaches for direct parametric image reconstruction in emission tomography. Med Phys 35:3963–3971
Turkheimer FE, Banati RB, Visvikis D, Aston JA, Gunn RN, Cunningham VJ (2000) Modeling dynamic PET-SPECT studies in the wavelet domain. J Cereb Blood Flow Metab 20:879–893
Van Laere K, Zaidi H (2006) Quantitative analysis in functional brain imaging. In: Zaidi H (ed) Quantitative analysis of nuclear medicine images. Springer, New York, pp 435–470
Vander BT, Minoshima S, Giordani B, Foster NL, Frey KA, Berent S, Albin RL, Koeppe RA, Kuhl DE (1997) Cerebral metabolic differences in Parkinson's and Alzheimer's diseases matched for dementia severity. J Nucl Med 38:797–802
Vaska P, Woody CL, Schlyer DJ, Shokouhi S, Stoll SP, Pratte J-F, O'Connor P, Junnarkar SS, Rescia S, Yu B, Purschke M, Kandasamy A, Villanueva A, Kriplani A, Radeka V, Volkow N, Lecomte R, Fontaine R (2004) RatCAP: miniaturized head-mounted PET for conscious rodent brain imaging. IEEE Trans Nucl Sci 51:2718–2722
Watabe H, Channing MA, Der MG, Adams HR, Jagoda E, Herscovitch P, Eckelman WC, Carson RE (2000) Kinetic analysis of the 5-HT2A ligand [11C]MDL 100,907. J Cereb Blood Flow Metab 20:899–909
Watabe H, Jino H, Kawachi N, Teramoto N, Hayashi T, Ohta Y, Iida H (2005) Parametric imaging of myocardial blood flow with 15O-water and PET using the basis function method. J Nucl Med 46:1219–1224
Watabe H, Ikoma Y, Kimura Y, Naganawa M, Shidahara M (2006) PET kinetic analysis–compartmental model. Ann Nucl Med 20:583–588
Wilson AA, Ginovart N, Schmidt M, Meyer JH, Threlkeld PG, Houle S (2000) Novel radiotracers for imaging the serotonin transporter by positron emission tomography: synthesis, radiosynthesis, and in vitro and ex vivo evaluation of (11)C-labeled 2-(phenylthio)araalkylamines. J Med Chem 43:3103–3110
Woody C, Vaska P, Schlyer D, Pratte J-F, Junnarkar S, Park S-J, Stoll S, Purschke M, Southekal S, Kriplani A, Krishnamoorthy S, Maramraju S, Lee D, Schiffer W, Dewey S, Neill J, Kandasamy A, O'Connor P, Radeka V, Fontaine R, Lecomte R (2007) Initial studies using the RatCAP conscious animal PET tomograph. Nucl Instr Meth A 571:14–17
Wu HM, Hoh CK, Choi Y, Schelbert HR, Hawkins RA, Phelps ME, Huang SC (1995) Factor analysis for extraction of blood time-activity curves in dynamic FDG-PET studies. J Nucl Med 36:1714–1722
Zaidi H, Montandon M-L (2006) The new challenges of brain PET imaging technology. Curr Med Imag Rev 2:3–13
Zhou Y, Ye W, Brasic JR, Wong DF (2010) Multi-graphical analysis of dynamic PET. Neuroimage 49(4):2947–2957